Journal of Advanced Mechanical Design, Systems, and Manufacturing

Vol. 3, No. 2, 2009

Influence of Design Parameters on Mechanical Power Losses of Helical Gear Pairs*

Sheng LI**, Aarthy VAIDYANATHAN**, Jonny HARIANTO**
and Ahmet KAHRAMAN**
**Gear and Power Transmission Research Laboratory
The Ohio State University, Columbus, OH 43210, USA
E-mail: kahraman.1@osu.edu

Abstract

In this study, the influence of basic design parameters and tooth surface modifications on the mechanical (friction induced) power losses of a helical gear pair is studied. A helical gear mechanical efficiency model based on elastohydrodynamic lubrication (EHL) is introduced. The model is used to simulate the gear contact conditions of an example helical gear pair within the ranges of basic design parameter such as pressure and helix angles, number of teeth (module), and major diameters to quantify their impact on mechanical power losses. Variation of gear efficiency with these parameters are then weighed against other functional requirements such as transmission error amplitudes, and contact and bending stresses to demonstrate that many designs that have high efficiency might perform poorly in terms of noise, pitting, and tooth breakage. A representative design that is acceptable in all aspects is considered next with varying amounts of tooth modifications to demonstrate their impact on power losses. At the end, recommendations are made on how to reduce helical gear mechanical power losses while meeting other functional requirements as well.

Key words: Helical Gear Power Losses, Gear Mechanical Efficiency, Gear Design

1. Introduction

Power losses at gear mesh interfaces of automotive drive train systems such as transmissions, transfer cases and axles represent a sizable portion of overall losses. While a helical gear pair could already be considered as a highly efficient power transmission component with mechanical efficiencies often exceeding 99.5% [(1)(2)], these losses multiply to sizable amounts in multi-stage arrangements. Under such conditions, minimizing power losses of the transmission requires a design methodology that considers efficiency as a requirement together with others regarding noise and durability (including pitting and tooth bending failure modes). Such a methodology would not only quantify the impact of basic design parameters on mechanical power losses of helical gear trains but also allow one to weigh efficiency against noise and durability to achieve a product that is balanced in all aspects. This paper focuses on development of such a methodology.

Several published studies focused on losses at the gear meshes, considering mostly spur gears [(3)-(11)]. These models either assumed a constant or empirically determined friction coefficient μ. Some of them computed μ from an EHL model for smooth surfaces. Xu et al [(2)] showed that accuracy of these models were limited to the empirical μ formula used and developed a hybrid helical gear mechanical efficiency model that uses a customized gear contact friction formula developed up-front by using EHL theory instead of relying on real-time EHL simulations. They used the EHL model of Cioc et al [(12)] to perform a large design of experiment for a particular gear oil of interest (75W90) including gear specific

*Received 17 Mar., 2009 (No. 09-0112)
[DOI: 10.1299/jamdsm.3.146]

ranges of key parameters such as temperature, normal load, rolling speed, sliding ratio, radii of curvature and surface roughness amplitude. They reduced the predicted surface traction data into a single μ formula using the linear regression technique. In addition, they coupled their efficiency model with a computationally efficient load distribution model [13] to perform gear mechanical power loss predictions in less than a second. Xu et al [2] showed this hybrid approach gives the same results as the real-time EHL runs in the simulation and compares well to the published gear power loss experiments [1].

The model of Xu et al [2] was limited to gear contacts that has no or limited asperity interactions due to the type of the EHL model used. Most automotive gears have reasonably large surface roughness originating from shaving or grinding processes and operate under low speed, heavy load and high temperature conditions with lubricants that are suboptimal, such that mixed EHL conditions with severe metal-to-metal contacts are common. Hence, the first objective of this study is to develop a new mixed EHL model and incorporate with the modeling methodology proposed earlier [2] to obtain an accurate mechanical efficiency model for spur and helical gear pairs. The second objective is to utilize the proposed gear power loss model to (i) identify and quantify the influence of key gear design parameters impacting efficiency, (ii) demonstrate simultaneous influence of the same parameters on transmission error and gear stresses, and (iii) obtain well-balanced designs that are acceptable in all aspects (efficiency, durability and noise) instead of being the best for any given attribute at the expense of others. These good solutions will then be refined further through profile modifications to quantify the combined influence of micro-geometry on the gear stresses, noise metrics and mechanical efficiency.

2. Gear Pair Mechanical Power Loss Methodology

The mechanical power loss methodology shown in Fig. 1 [2] relies on three main modules: (i) a gear load distribution module [13], (ii) an EHL-based friction coefficient computation module, and (iii) a gear pair mechanical power loss computation module. The load distribution model predicts the contact stress distribution of a helical gear pair with or without certain manufacturing and assembly errors as well as profile modifications. It also yields sliding and rolling velocities and radii of curvature at the contact zones of the gear mesh. These parameters are fed into a friction coefficient model to find the instantaneous

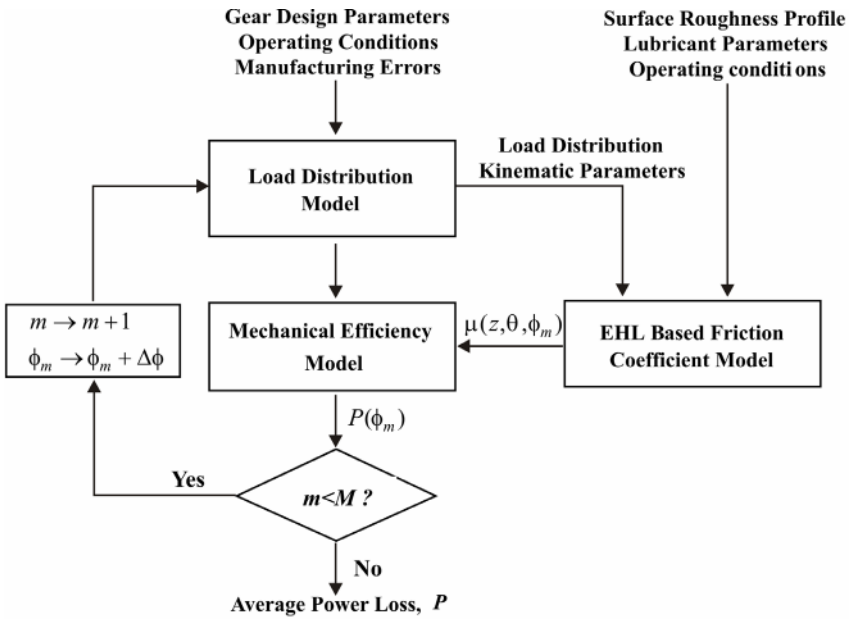

Fig. 1 Helical gear mechanical power loss computation methodology [2]

friction coefficient $\mu(z,\theta,\phi_m)$ of every contact point (z,θ) on the gear tooth surfaces at each roll angle position ϕ_m. Next, $\mu(z,\theta,\phi_m)$ is used by the mechanical power loss module to determine the instantaneous efficiency $P(\phi_m)$ of the gear pair at the m-th incremental rotational position. The above sequential procedure is repeated for an M number of discrete positions ($m \in [1, M]$) spaced at an increment of $\Delta\phi$ ($\phi_m = m\,\Delta\phi$) that covers a complete mesh cycle [2].

For the computation of the contact loads of helical gears, a load distribution model (LDP) that is initially proposed by Conry and Seireg [13] is used in this study. This model computes elastic deformations at any point of the gear surface, given the tooth compliance, applied torque, and the initial unloaded tooth separations. For the solution of the gear contact problem, conditions of compatibility and equilibrium are considered. The condition of compatibility ensures for any point within the contact zone that the sum of elastic deformations of two bodies and the initial separation are greater than or equal to the rigid body displacement. The condition of equilibrium states that the sum of the moments applied on a gear body must be equal to zero. With these two conditions in hand, the load distribution problem is solved iteratively by using a modified Simplex algorithm for the values of the unknown force vector.

2.1 Computation of the Friction Coefficient

By discretizing a helical gear pair into a number of thin slices of spur gears that are staggered according to the helix angle, the contact on each slice pair can be modeled as a line contact between two cylinders of radii of curvature r_1 and r_2 and surface velocities $u_1 = r_1\omega_1$ and $u_2 = N_1 r_2 \omega_1 / N_2$ where N_1 and N_2 are the numbers of teeth of gears 1 and 2 and ω_1 is the rotational speed of gear 1 in rad/s. This contact segment has a normal load W predicted by the load distribution model. For this lubricated contact, the transient Reynolds equation governs the non-Newtonian fluid flow in the contact areas with no asperity interactions

$$\frac{\partial}{\partial x}\left[f \frac{\partial p}{\partial x} \right] = \frac{\partial (u_r \rho h)}{\partial x} + \frac{\partial (\rho h)}{\partial t} \tag{1.a}$$

where the parameters p, h and ρ denote the pressure, thickness and density of the fluid, respectively, all of which are dependent on x and t, and $u_r = (u_1 + u_2)/2$ is the rolling velocity. The fluid flow coefficient is defined as [14]

$$f = \frac{\rho h^3}{12\eta} \cosh\left(\frac{\tau_m}{\tau_0} \right) \tag{1.b}$$

where η is the lubricant viscosity, τ_0 is any lubricant reference stress, and the viscous shear stress $\tau_m = \tau_0 \sinh^{-1}\left[\eta u_s / (\tau_0 h) \right]$. Here, $u_s = u_1 - u_2$ is the sliding velocity of the contact. Equation (1) describes the lubricant flow within the contact regions where the fluid film thickness is greater than zero such that the surfaces are separated. In the regions where the asperity contact occurs ($h = 0$), the Reynolds equation is set to [15]

$$\frac{\partial (u_r \rho h)}{\partial x} + \frac{\partial (\rho h)}{\partial t} = 0 \tag{2}$$

Assuming a smooth transition between the fluid and asperity contact areas, Eq. (1) and (2) constitute a "unified" Reynolds equation system that governs the mixed EHL behavior of the contact, considering both the fluid and the asperity contact regions simultaneously.

The film thickness at a contact point of any coordinate x and time t under elastic conditions is defined as

$$h(x,t) = h_0(t) + g_0(x) + V(x,t) - R_1(x,t) - R_2(x,t) \tag{3}$$

where $h_0(t)$ is the reference film thickness, and $R_1(x,t)$ and $R_2(x,t)$ are the roughness profiles of the two surfaces at time t. Here, $R_1(x,t)$ and $R_2(x,t)$ move at velocities of u_1 and u_2 that correspond to a slide-to-roll ratio $SR = u_s/u_r = 2(u_1 - u_2)/(u_1 + u_2)$. The term $g_0(x)$ is the geometric gap between the two surfaces that is given as a function of the equivalent radius of curvature $r_{eq} = r_1 r_2/(r_1 + r_2)$ and the x coordinate in the direction of sliding as $g_0(x) = x^2/(2r_{eq})$. The elastic deformation $V(x,t)$ due to the normal load W applied is given as [16]

$$V(x,t) = \int_{x_s}^{x_e} K(x-x')p(x',t)dx' \tag{4}$$

where $K(x) = -4\ln|x|/(\pi E')$ is the influence coefficient with $E' = 2\left[(1-\upsilon_1^2)/E_1 + (1-\upsilon_2^2)/E_2\right]^{-1}$ where υ_i and E_i are the Poisson's ratio and the Young's modulus of contact body i.

A two-slope viscosity-pressure model is used here [17]

$$\eta = \begin{cases} \eta_0 \exp(\alpha_1 p), & p < p_a, \\ \eta_0 \exp(c_0 + c_1 p + c_2 p^2 + c_3 p^3), & p_a \le p \le p_b, \\ \eta_0 \exp\left[\alpha_1 p_t + \alpha_2 (p - p_t)\right], & p > p_b, \end{cases} \tag{5}$$

where α_1 and α_2 are the viscosity-pressure coefficients for the low ($p < p_a$) and high ($p > p_b$) pressure ranges, respectively, p_t is the transition pressure value between these two ranges, and p_a and p_b are the threshold pressure values of the low and high pressure ranges, respectively. In addition, the density-pressure relationship can be defined as [18]

$$\rho = \rho_0 \frac{(1+\gamma p)}{(1+\lambda p)} \tag{6}$$

where $\gamma = 2.266\times10^{-9}$ Pa^{-1} and $\lambda = 1.683\times10^{-9}$ Pa^{-1}. The last equation of interest here is the load balance equation, which is used to check whether the total contact force due to the pressure distribution (both hydrodynamic and asperity contact) over the entire contact area is balanced by the normal tooth load applied at that instant

The computational domain for the mixed EHL analysis is defined as $-2.5a \le x \le 1.5a$, where a is the half width of the corresponding Hertzian contact zone. In order to capture the surface roughness geometry sufficiently, a sufficiently fine contact grid mesh consisting of N grid elements is used. At a given time increment t_n, the lubricant viscosity, density, film thickness, and pressure are all assumed to be uniform within each contact element i ($i \in [1, N]$), represented by the values at the center of the grid cell. Considering an asymmetric control volume, Eqs. (1)~(6) are discretized to obtain a numerical solution.

The surface shear traction consists of the viscous shear exerted by the lubricant within the lubricated regions and the asperity friction force results from the metal-to-metal contacts within the boundary lubrication regions. The viscous shear stress acting on surface 1 is defined as

$$q = -\frac{h}{2}\left(\frac{\partial p}{\partial x}\right) + \eta_x^* \frac{(u_2 - u_1)}{h} \tag{7}$$

where $\eta_x^* = \eta/\cosh(\tau_m/\tau_0)$ is the effective viscosity in the direction of rolling. Within the asperity regions, the shear stress is defined as $q = \mu_d p$, where μ_d is the coefficient of friction for dry contact condition. With these, the friction coefficient at a given time instant t_n is

$$\mu_{t_n} = \frac{1}{W'} \int_{x_s}^{x_e} q(x, t_n) dx. \tag{8}$$

where W' is load per unit face width. Each simulation is carried out for a total of N_t time steps and the average friction coefficient for the contact condition considered is defined as $\mu = \sum_{n=1}^{N_t} \mu_{t_n} / N_t$.

Here, instead of using the mixed EHL model directly in real time to determine the traction force at every contact cell on the tooth surface, an up front parametric study is performed by considering all combinations of the key parameter values. Here, ranges suitable for automotive gears are defined for each key parameter p_h ($0.5-2.5$ GPa), r_{eq} ($5-80$ mm), u_r ($1-20$ m/s), SR ($0-1$), and viscosity through oil temperature ranging from $25\ ^\circ C$ to $100\ ^\circ C$. In addition, a measured roughness profile from a shaved gear surface with $R_q = 0.5$ μm is considered and different RMS roughness profiles with different amplitudes are obtained from this baseline profile by multiplying it by a constant. A typical automatic transmission fluid is used as the example lubricant.

A total of 42,000 combinations covering a wide range of contact conditions experienced by automotive gearing are obtained from the parameter values listed above. The predicted μ values for these combinations are plotted against the lambda ratio $\bar{\lambda}$ (ratio of the minimum film thickness calculated by using Dowson-Higginson formula for line contacts [18] to the RMS surface roughness value) to reveal a piecewise linear relationship as shown in Fig. 2. Here, linear scales are used for $\bar{\lambda}$ and μ to show that there is a two-slope piecewise-linear relationship between them for a majority of the contact conditions. For $\bar{\lambda} \le 1$, μ varies quite linearly with $\bar{\lambda}$ with a very steep negative slope representing the boundary or mixed EHL conditions, while another linear relation with much smaller negative slope is observed for $\bar{\lambda} > 1$ when there is little of no asperity interactions. The histogram of the entire friction coefficient data points to two different populations, indicating that any curve fitting effort must treat the data for $\bar{\lambda} > 1$ and $\bar{\lambda} \le 1$ separately. With these the EHL μ data of this parametric study is divided into two subsets at the threshold value of $\bar{\lambda} = 1$, and a regression analysis is carried out for each subset separately. The first order parameters selected for the general linear regression model for the response parameter of $\ln \mu$ are $\bar{W} = -\log_{10}(p_h / E')$, $\bar{\alpha} = \log_{10}(\alpha_1 E')$, $\bar{r}_{eq} = \log_{10}(r_{eq} E' / W')$, $\bar{V} = -\log_{10}[u_r \eta_0 / W']$, $\bar{\lambda}$, SR and two roughness parameters $\bar{S}_c = S_c E' / W'$ and $\bar{S}_{eq} = S_{eq} E' / W'$. Here, $W' = W / L$ is the load density along the contact line of length L, $S_c = \sqrt{R_{q1}^2 + R_{q2}^2}$ and $S_{eq} = R_{q1} R_{q2} / (R_{q1} + R_{q2})$. In addition, the higher order parameters, which are the combination of those first order parameters, are also considered. Utilizing the statistical software, MINITAB, the following regressed μ formula is obtained with an adjusted R-square value of about 92%:

For $\bar{\lambda} \le 1$:

$$\mu = \exp\left[a_0 + a_1 \bar{\lambda} \bar{S}_c + a_2 \bar{W} \bar{r}_{eq} + a_3 \bar{\lambda}^{\bar{W}} + a_4 \bar{S}_{eq}^{\bar{\lambda}} \right] (SR)^{a_5 \bar{\lambda}} \bar{S}_{eq}^{a_6 \bar{\lambda}} \bar{S}_c^{\left[a_7 (SR) + a_8 \bar{V} + a_9 \ln \bar{\lambda} \right]} \tag{9.a}$$

For $\bar{\lambda} > 1$:

$$\mu = \exp\left[b_0 + \bar{\lambda}(b_1 \bar{V} + b_2 \bar{r}_{eq}) + b_3 \bar{V}^{\bar{r}_{eq}} + b_4 \bar{\alpha}^{\bar{W}} + b_5 \bar{\alpha}^{\bar{r}_{eq}} + b_6 \bar{r}_{eq}^{\bar{V}} \right] \bar{\lambda}^{(b_7 + b_8 \bar{V})} (SR)^{\left[b_9 + b_{10} \ln \bar{\lambda} + b_{11} \bar{\alpha} \right]} \bar{W}^{b_{12} \bar{\lambda}} \bar{S}_c^{b_{13} \bar{\lambda}} \tag{9.b}$$

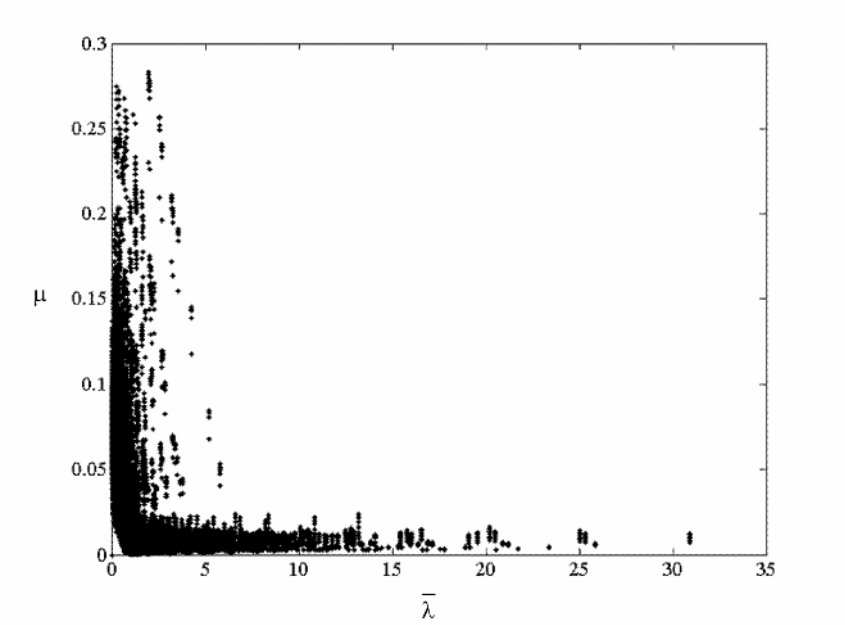

Fig. 2 Variation of μ with $\bar{\lambda}$ for all the contact combinations considered

Here, coefficients $a_0 - a_9$ and $b_0 - b_{13}$ are constants representative of the lubricant considered.

2.2 Computation of Gear Pair Mechanical Power Losses

Once the friction coefficient $\mu(z,\theta,\phi_m)$ at each contact point (z,θ) at each rotational angle ϕ_m ($m = 1,2,\ldots,M$) are known, the friction force at each contact position can be calculated via

$$F_f(z,\theta,\phi_m) = \mu(z,\theta,\phi_m) W(z,\theta,\phi_m) \tag{10}$$

where $W(z,\theta,\phi_m)$ is the normal load at the contact point of interest. The instantaneous mechanical power loss and the mechanical efficiency of the gear are given as

$$P(\phi_m) = \sum_{q=1}^{Q} \left[\mu W u_s\right]_q , \qquad \eta(\phi_m) = 1 - \frac{P(\phi_m)}{T_{in}\omega_{in}} \tag{11.a,b}$$

where Q is the total number of loaded contact segments at mesh position ϕ_m, T_{in} is the input torque, and ω_{in} is the input speed. These instantaneous values are averaged over an entire mesh cycle to find the average gear mesh mechanical power loss and mechanical efficiency as $P = \frac{1}{M}\sum_{m=1}^{M} P(\phi_m)$ and $\eta = 1 - P/(T_{in}\omega_{in})$.

3. A Parameter Sensitivity Study

The efficiency model proposed in the previous section was validated this efficiency model in two levels. First, the EHL model predictions and the resultant friction coefficient formula, Eq. (9), were compared to twin-disk and ball-on-disk traction measurements to show that they are indeed accurate within the ranges of load, rolling and sliding velocity and surface roughness amplitudes. Comparisons between the gear mesh power loss predictions of proposed model and experiments of Petry-Johnson et al. [1] were also made to show that the predictions are typically within 0.1 kW of measurements.

The proposed helical gear mechanical efficiency model will be used here to perform an example design study. The predicted parameters in this study will include peak-to-peak transmission error (*TE*) as a noise metric, and maximum contact and root bending stresses (σ_c and σ_b) as gear fatigue life metrics. In addition, the mechanical power loss *P* is computed using the proposed model to represent the efficiency of the gear design. The ultimate goal here is to find a design that results in minimum values for all of *P*, *TE*, σ_c, and σ_b.

An example condition with a fixed center distance of 91.5 mm and unity (1:1) ratio is considered here. Both gears of the pair (gear and pinion) are kept identical to reduce the number of parameters. In addition, the face width of all gears was kept constant at 25 mm. Four basic gear design parameters, normal pressure angle (Φ), helix angle (Ψ), the number of teeth (*N*) and the working depth ratio (Λ_{wd}) are varied. The working depth constant is defined here as the ratio of the sum of addendum and dedendum of the gears to normal module (*m*). Λ_{wd} is varied between 1.85 and 3.38 at an increment of 0.218 (8 levels) to obtain a range of tooth heights. Meanwhile, *N* is varied from 20 to 53 with an increment of 1 to represent a range of fine to coarse gear teeth. Discrete values between 15 and 30 degrees are considered for both Φ (increment of 2.5 deg) and Ψ (increment of 1 deg). A profile crown of $M_P = 15$ μm and a lead crown of $M_L = 12$ μm are applied to all of the gears. An automatic transmission fluid at $90^\circ C$ is used in the simulations. Input torque and speed are kept at $T_{in} = 250$ Nm and $\Omega_{in} = 60\omega_{in}/2\pi = 4000$ rpm. The surface roughness amplitudes of the gears are $R_{q1} = R_{q2} = 0.4$ μm.

All combinations of values of all four parameters specified above resulted in more than 30,000 different designs, of which only 13,500 deemed acceptable as the rest were eliminated due to reasons such as inadequate backlash, tip thickness or root clearance (minimum acceptable backlash, tip thickness and root clearance values were chosen as 0.04, 0.2 and 0.2).

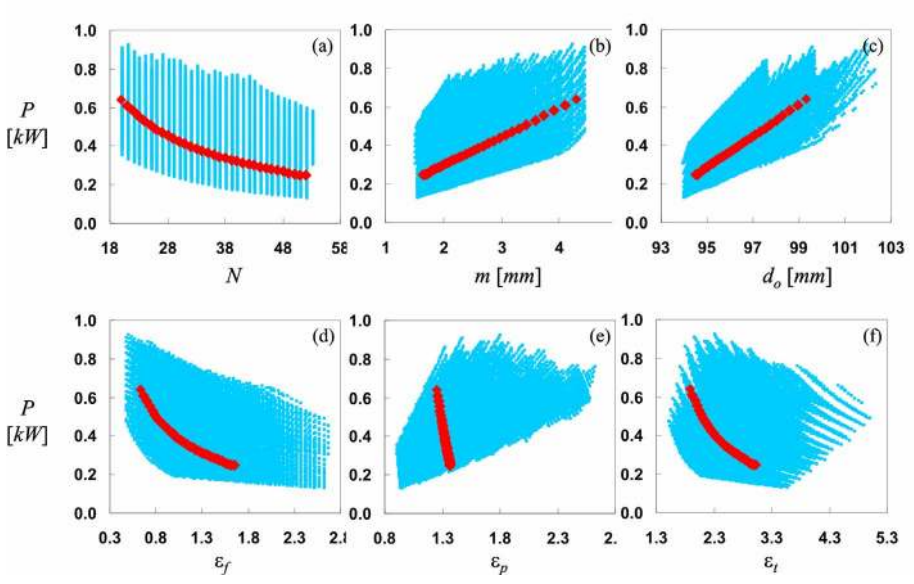

Fig. 3 Variation of *P* with (a) *N*, (b) *m*, (c) d_o (d) ε_f, (e) ε_p, and (f) ε_t. The vertical scales of the charts in the first column apply to the respective charts in the other two columns as well.

In Fig. 3(a-c), the variation of the mechanical power loss P of all of the 13,500 designs are plotted against N, m and Λ_{wd}, respectively (small lighter color dots). In Fig. 3(a), about a 0.3 to 0.6 kW spread in P is observed for each N value due to variations coming from the other parameter ranges. In general, P tends to reduce with increase in number of teeth. When the other parameters are fixed at $\Phi = 22.5^\circ$, $\Psi = 20^\circ$ and $\Lambda_{wd} = 2.286$, the database is reduced to 32 designs represented by larger symbols in Fig. 3(a). This subset of data points shows the sole influence of N on P. Along the curve formed by these data points, $P \approx 0.6$ kW for $N = 20$ teeth, which is reduced to half when the number of teeth is increased to 50. This suggests that finer pitch gears should have lower mechanical power losses as observed experimentally [1] and theoretically [2]. Figure 3(b) that plots P against normal module m supports the same conclusion in an even more convincing way. The 13,500 designs consider cover a module range of 1.5 to 4.4 mm. Again focusing on the subset of data with $\Phi = 22.5^\circ$, $\Psi = 20^\circ$ and $\Lambda_{wd} = 2.286$, an almost linear relationship between P and m is observed in Fig. 3(b) obtained by changing N. In Fig 3(c), meanwhile, variation of P with the major (outside) diameter d_o of gears is illustrated. The general trend observed from the larger population is that P increases with d_o. In other words, longer teeth that result in more sliding increases power losses as well. Looking at the same sub-set of the data as Fig. 3(a,b), P is shown to increase in linear manner with d_o, changing from 0.25 kW at $d_o = 94$ mm to 0.6 kW at $d_o = 99$ mm. Figures 3(d-f) show the variation of P with face, profile and total contact ratios ($\varepsilon_t = \varepsilon_f + \varepsilon_p$). Here, there is no apparent trend between P and ε_f and ε_p. This is because these contact ratios can be changed in different ways that might cause reductions or increases in P. For instance, ε_p can be increased conveniently by reducing module as well as increasing the major diameter of gears. The former was shown in Fig 3(b) to reduce the P while the latter in Fig 3(c) was shown to increase it. As a result, the 13,500 designs plotted in Fig. 3(e) do not follow a trend. Meanwhile, the same subset of the data with $\Phi = 22.5^\circ$, $\Psi = 20^\circ$ and $\Lambda_{wd} = 2.286$ (larger symbols) indicate that P reduces with both ε_f and ε_p, influence of ε_p being more drastic.

Figure 4(a) plots P versus normal pressure angle Φ, suggesting that an increase in Φ helps reduce P. Defining a sub-set of the data with $N = 30$ teeth, $\Psi = 20^\circ$ and $\Lambda_{wd} = 2.286$, the same figure also shows the variation of this group of designs with Φ. This subset of data shows that P is reduced from almost 0.8 kW to 0.4 kW by increasing Φ from 15° to 25°. The same trend is observed in Fig. 4(b) for Ψ, but now in a less significant way. On the same figure, it was also shown that increasing Ψ from 15° to 30° for a group of candidate designs with $N = 30$ teeth, $\Phi = 22.5^\circ$ and $\Lambda_{wd} = 2.286$ reduces P by only about 20%. Finally, in Fig. 4(c), the sole influence of Λ_{wd} is illustrated, with a sub-set formed by designs having $N = 30$, $\Phi = 22.5^\circ$ and $\Psi = 20^\circ$ showing a sizable increase in P with Λ_{wd}.

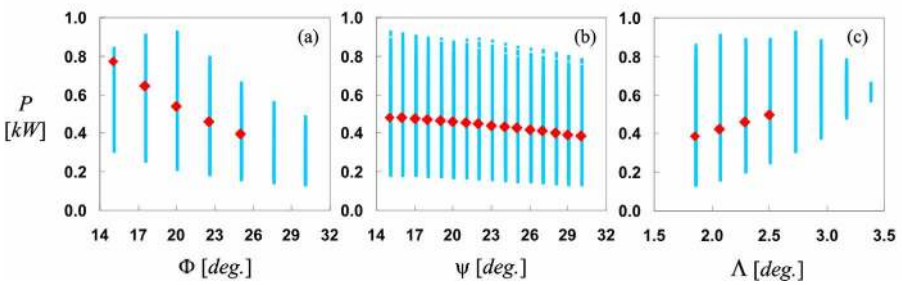

Fig. 4 Variation of P with (a) Φ, (b) Ψ, and (c) Λ_{wd}.

Figures 3 and 4 reveal certain trends that help reduce P such as increasing Φ or

reducing d_o. Some of these trends can be expected to increase noise excitations while hurting the contact and bending stresses as well. In other words, a design that is very good for power loss characteristics might indeed be very poor for its other attributes. In order to illustrate this, the same 13,500 designs were evaluated for their peak-to-peak transmission error (*TE*), and maximum contact and root bending stresses (σ_c and σ_b) as shown in Fig. 5(a-c). In Fig. 5(a), *P* versus *TE*, we choose a candidate Design A (see Table 1 for its parameters) that is has the lowest *P* and *TE* values (i.e. most efficient and potentially the quietest design). The same Design A is also located in Fig. 5(b,c) to show its σ_c and σ_b values. It is clear here that design A is rather marginal in terms of σ_c and it is absolutely one of the worst designs in terms of its bending strength as it has a very high σ_b value. Similarly, in Fig. 5(c), we choose a Design B based on combined *P* and σ_b as a favorable design and locate the same design in Fig. 5(a,b) to show that it has very high *TE* value. Similarly, Design C that is good for *P* and σ_c in Fig. 5(b) is shown to have very high σ_b. This indicates clearly that the selection of a design that is good in all attributes is complex engineering trade-off. Using the methodology proposed here, one can sort the database of candidate design to identify a design that is acceptable on all five attributes *P*, *TE*, σ_c and σ_b while it might not necessarily be the best in any single attribute. Design D marked in Fig. 5 (and listed in Table 1) represent such a design. This design was obtained by searching the 13,500 candidate designs such that $P < 0.3$ kW, $\sigma_b < 235$ MPa, $\sigma_c < 1.175$ GPa, and the peak-to-peak $TE < 0.25$ μm.

The entire candidate designs used in Figs. 3-5 used a profile crown of $M_P = 15$ μm and a lead crown of $M_L = 12$ μm. Input torque and speed was kept at $T_{in} = 250$ Nm. Design D from Fig. 5 and Table 1 will be used next to determine the combined influence of tooth modifications in the form of M_P and M_L, and T_{in} on the efficiency, noise and durability metrics. Tooth modification studies are performed by varying M_P and M_L between 0 and 30 μm for various T_{in} values. Figure 6(a) shows variation of *P* with M_P and M_L at three of these discrete T_{in} values. Data point D from Fig. 5(a) is also marked in this figure. Here, regardless of T_{in}, increases in M_P help reduce *P* with severe consequences on *TE* as shown in Fig. 6(b). Likewise, the corresponding σ_c and σ_b in Fig. 6(c) and (d) are shown to increase with M_P and M_L, further suggesting that the efficiency concerns must be balanced by the other attributes in defining tooth modification.

4. Conclusions

The influence of basic design parameters and tooth surface modifications on the mechanical (friction induced) power losses of a helical gear pair was studied. A helical gear mechanical efficiency model based on a mixed EHL lubrication formulations was proposed and used to simulate the gear contact conditions of an example helical gear pair within ranges of pressure and helix angles, numbers of teeth (module), and working depth ratio to assess their impact on mechanical efficiency. Combined influences these parameters on power losses were then weighed against transmission error amplitudes, and contact and bending stresses to indicate that many designs that have high efficiency might perform poorly in terms of noise and durability. A multi-torque tooth modification study was performed at the end by using a design that is equally good in various aspects to show that similar contradictions appear in terms of selection of the tooth modifications as well. The proposed helical gear mechanical efficiency model is very computationally efficient allowing its use as a tool to aid a gear designer to include gear efficiency as a requirement in the development of the gear systems.

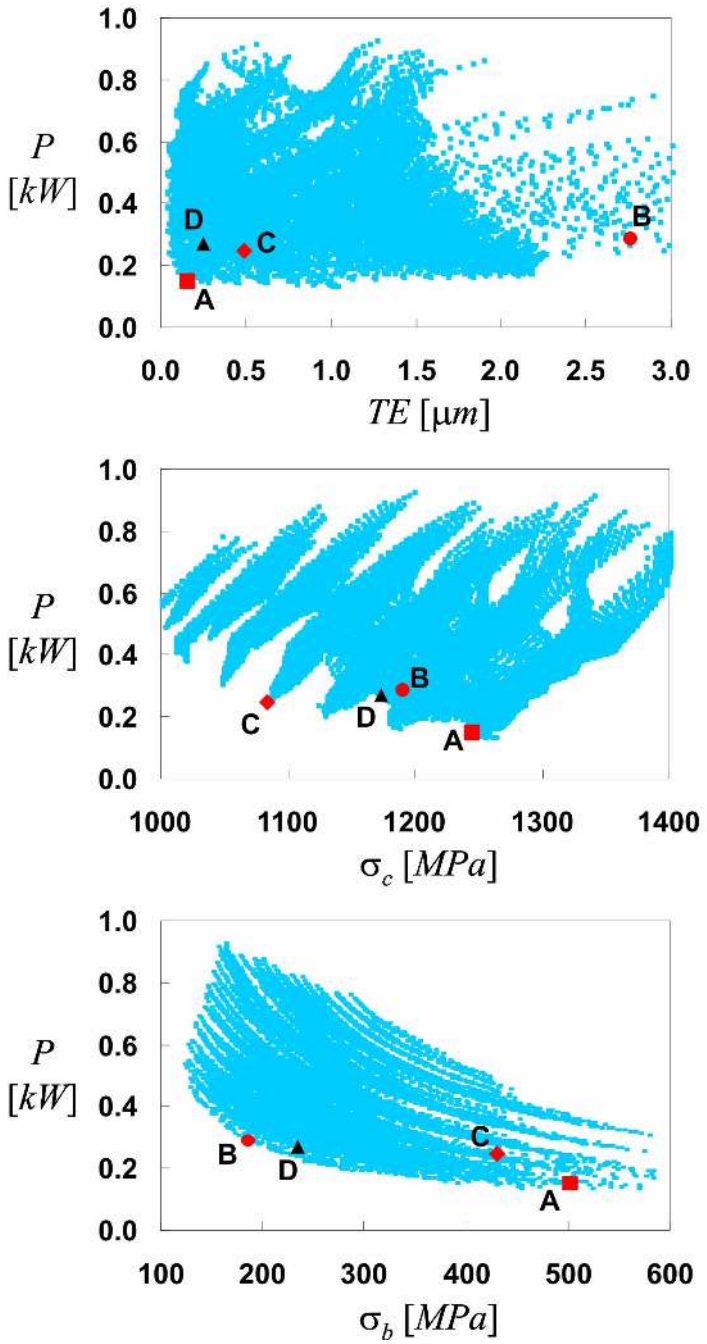

Fig. 5 Variation of P against (a) peak-to-peak TE, (b) maximum σ_c, and (c) maximum σ_b.

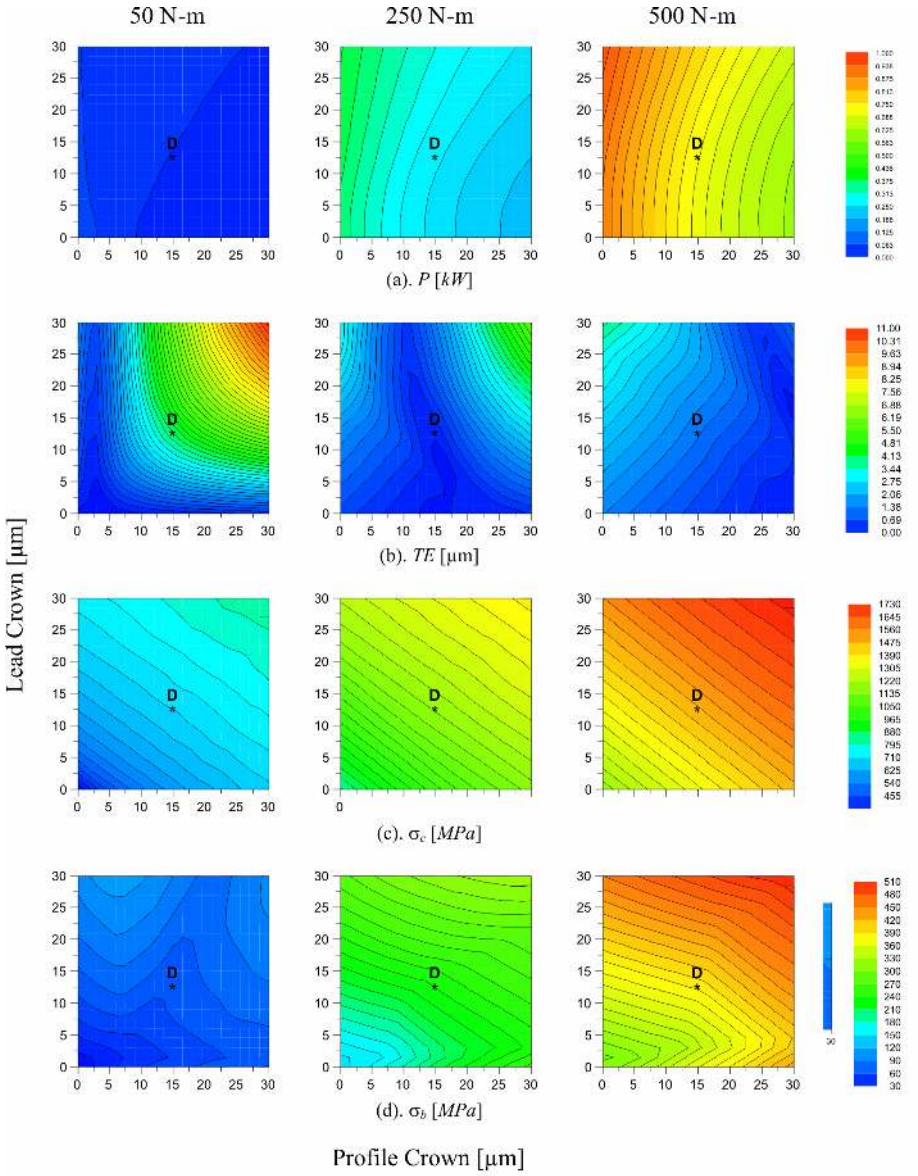

Fig. 6 Variation of (a) *P*, (b) *TE*, (c) σ_c and (d) σ_b with the profile crown M_P and lead crown M_L at $T_{in} = 50$, 250 and 500 Nm.

Parameter	Candidate Designs A	B	C	D
N	49	28	49	32
Φ [*deg*]	30	30	22.5	30
Ψ [*deg*]	27	19	30	19
Λ_{wd}	1.85	1.85	2.504	2.068
d_o [*mm*]	94.16	96.44	95.15	96.42
Root diameter [*mm*]	88.01	85.01	87.05	85.23
m [*mm*]	1.6638	3.0898	1.6172	2.7036
Face width [*mm*]	25	25	25	25

Table 1 Gear parameters of 4 designs identified in Fig. 4

References

(1) Petry-Johnson, T., Kahraman, A., Anderson, N.E. and Chase, D., An experimental and theoretical investigation of power losses of high-speed spur gears, *Journal of Mechanical Design*, Vol. 130 (2008).
(2) Xu, H., Kahraman, A., Anderson, N.E. and Maddock, D., Prediction of mechanical efficiency of parallel-axis gear pairs, *Journal of Mechanical Design*, Vol. 129 (2007), pp. 58-68.
(3) Pedrero, J. I., Determination of the efficiency of cylindrical gear sets, *4th World Congress on Gearing and Power Transmission*, Paris, France, (1999).
(4) Michlin, Y. and Myunster,V., Determination of power losses in gear transmissions with rolling and sliding friction incorporated, *Mechanism and Machine Theory*, Vol. 37 (2002), pp. 167.
(5) Anderson, N. E. and Loewenthal, S. H., Design of spur gears for improved efficiency, *Journal of Mechanical Design*, Vol. 104 (1982), pp. 767-774.
(6) O'Donoghue, J. P. and Cameron, A., Friction and temperature in rolling sliding contacts, *ASLE Transactions*, Vol. 9 (1966), pp. 186-194.
(7) Drozdov, Y. N. and Gavrikov, Y. A., Friction and scoring under the conditions of simultaneous rolling and sliding of bodies, *Wear* (1967), pp. 291-302.
(8) Martin, K. F., The efficiency of involute spur gears, *Journal of Mechanical Design*, Vol. 103 (1981), pp. 160-169.
(9) Simon, V., Load capacity and efficiency of spur gears in regard to thermo-end lubrication, *International Symposium on Gearing and Power Transmissions*, Tokyo, Japan, (1981).
(10) Wu, S. and Cheng, H., S., A friction model of partial-EHL contacts and its application to power loss in spur gears, *Tribology Transactions*, Vol. 34, No. 3 (1991), pp.398-407.
(11) Mihalidis, A., Bakolas, V., Panagiotidis, K. and Drivakos, N., Predition of the friction coefficient of spur gear pairs, *VDI-Berichte*, NR. 1665 (2002), pp. 705-719.
(12) Cioc, C., Cioc, S., Kahraman, A and Keith, T., A non-Newtonian thermal EHL model of contacts with rough surfaces, *Tribology Transactions*, Vol 45 (2002), pp. 556-562.
(13) Conry, T. F., Seireg, A., A mathematical programming technique for the evaluation of load distribution and optimal modifications for gear systems, *ASME Journal of Engineering for Industry*, *Series B*, Vol. 95 (1973), pp. 1115-1122.

(14) Ehret, P., Dowson, D. and Taylor, C.M., On lubricant transport conditions in elastohydrodynamic conjunctions, *Proceedings of the Royal Society of London*, Series A, 454 (1998), pp.763–787.
(15) Hu, Y.Z., Wang, H., Wang, W.Z. and Zhu, D., A computer model of mixed lubrication in point contacts, *Tribology International*, 34 (2001), pp.65–73.
(16) Johnson, K. J., Contact Mechanics. Cambridge University Press, Cambridge, (1985).
(17) Goglia, P.R., Cusano, C. and Conry, T.F., The effects of surface irregularities on the elasto-hydrodynamic lubrication of sliding line contacts, part I – single irregularities, part II – Wavy surfaces, *ASME Journal of Tribology*, Vol. 106 (1984), pp.104–119.
(18) Dowson, D. and Higginson, G.R., Elasto-hydrodynamic Lubrication. Pergamon Press, (1977).